Origin of the large interfacial perpendicular magnetic anisotropy in MgO/Co₂FeAl

Sicong Jiang,[1,2] Safdar Nazir,[1] and Kesong Yang ●[1,2,3,*]

[1]*Department of NanoEngineering and Program of Chemical Engineering, University of California San Diego, La Jolla, California 92093-0448, USA*

[2]*Program of Materials Science and Engineering, University of California San Diego, La Jolla, California 92093-0418, USA*

[3]*Center for Memory and Recording Research, University of California San Diego, La Jolla, California 92093-0401, USA*

Interfacial perpendicular magnetic anisotropy in the MgO/Co₂FeAl heterostructure is desired for technological applications, while the origin of the large interfacial anisotropy constant K_i remains controversial. Here we show that, by modeling four types of interface models for the MgO/Co₂FeAl system using first-principles calculations, the MgO/Co₂ interface is energetically more favorable than the MgO/FeAl interface and the interfacial Co atoms at the former interface produce out-of-plane K_i, while the interfacial Fe atoms at the latter interface produce in-plane K_i. The origin of these different behaviors can be explained by the atomic-resolved and orbital-resolved K_i along with the perturbation theory energy analysis. In addition, we also studied the influence of 26 capping layers on the interfacial magnetic anisotropy of MgO/Co₂FeAl and found that Fe and W capping can significantly enhance K_i in the MgO/Co₂FeAl with a particularly large K_i of 4.90 mJ/m² in the W-capped model. This work clarifies the atomistic origin of the interfacial perpendicular magnetic anisotropy and provides guidance to further enhance interfacial K_i by adding capping layers in the MgO/Co₂FeAl.

I. INTRODUCTION

Magnetic tunnel junctions (MTJs) consisting of two ferromagnetic (FM) layers separated by a thin insulating barrier are core components in spin-transfer-torque magnetic random-access memory [1,2]. In particular, the perpendicular MTJs (p-MTJs) that possess perpendicular magnetic anisotropy (PMA) have attracted a great deal of attention in recent years because of their promising applications in the next-generation spintronic devices towards using faster and smaller magnetic bits [3–6]. In p-MTJs, PMA occurs at the interface between the ferromagnetic thin film and insulating barrier, and its strength is characterized by the magnetic anisotropy constant K_i, which is defined as the anisotropy energy per unit area [7]. To achieve a high thermal stability of the relative magnetization orientation of the two ferromagnetic electrodes, a large K_i is desired. As p-MTJs shrink to the nanometer scale, a larger K_i is necessary to sustain a sufficient thermal stability. A recent theoretical calculation indicated that a K_i of 4.7 mJ/m² is needed for a data retention time of 10 years when the memory devices scale down to 10 nm [8].

PMA has traditionally been achieved at interfaces between ferromagnetic and nonmagnetic heavy metals such as Co/Pt; however, their K_i is small (less than 1 mJ/m²) [9]. In 2010, a large K_i of 1.3 mJ/m² was reported at the MgO/CoFeB interface, and the MTJ based on this material interface exhibits a high tunnel magnetoresistance ratio of 120% and a low switching current of about 49 μA [5]. Since then, great research efforts have been made either to tune K_i at the MgO/Fe interface [7] or to explore the possibility of

producing large K_i at novel MgO-based interfaces [10,11]. Co₂FeAl, one prototype compound of the full Heusler family, has received increasing interest as one possible alternative to Fe and CoFeB in the MgO-based p-MTJs in recent years because of its excellent properties, including high spin polarization [12], a low magnetic damping constant (about 0.001) [13], and a small lattice mismatch [14] between the Co₂FeAl film and MgO substrate (∼4%). The magnetic anisotropy at the MgO/Co₂FeAl interface was first reported in 2011 and was found to be very sensitive to the annealing [10,11,15]. Jiang's team [15] and Inomata's team [10] both reported a PMA at the MgO/Co₂FeAl interface independently and found a magnetic anisotropy transition from in plane to out of plane after annealing [10]. In contrast, in-plane magnetic anisotropy was also found at the MgO/Co₂FeAl interface and showed different behavior with the annealing temperature [11,16]. A very recent experimental study also reported the evolution of PMA at the interface between MgO and Co₂FeAl, i.e., a K_i of zero for as-deposited samples and a K_i of 1.14 (2.01) mJ/m² for samples annealed at 320 °C (450 °C), which is attributed to the modification of the interface during the thermal treatment [17].

PMA is mainly determined by the magnetic ions of a few monolayers near the interfacial region, and there exist two types of interfaces in the MgO/Co₂FeAl heterostructure, i.e., MgO/Co₂ and MgO/FeAl. Accordingly, one may speculate that the different magnetic anisotropies are caused by the different interfacial terminations between the MgO substrate and Co₂FeAl film. Inomata's team investigated the PMA at the MgO/Co₂FeAl interface using angle-dependent x-ray magnetic circular dichroism (XMCD) and attributed the PMA mostly to the interfacial Fe atoms at the MgO/FeAl interface [18]. Later, the same team also argued that the PMA at the

*kesong@ucsd.edu

Co$_2$FeAl heterostructure is mainly contributed by the large perpendicular orbital magnetic moments of interfacial Fe ions from XMCD measurement [19]. A prior theoretical study indicated that oxygen-top FeAl termination has the highest thermal stability on the basis of density functional theory calculations [20], which seems to support the above arguments. However, a recent computational study indicated that the FeAl termination at the MgO/Co$_2$FeAl interface leads to an in-plane instead of out-of-plane magnetic anisotropy, while the Co termination showed PMA with K_i up to 1.31 mJ/m^2 [21]. Therefore, to clarify the atomistic origin of the magnetic anisotropy at the MgO/Co$_2$FeAl interface, a comprehensive study of the interfacial magnetic properties and an evaluation of the relative thermodynamic stability of the two types of material interfaces are very necessary.

Additionally, a series of recent experimental and computational studies indicated that metal-based capping layers have a significant influence on K_i of the MgO/Co$_2$FeAl heterostructure [22,23], in which capping layers are often used to protect the ferromagnetic layers. For instance, Cr-capped MgO/Co$_2$FeAl showed an in-plane magnetic anisotropy with a K_i of -0.46 mJ/m^2, while a Ta-capped film exhibited a PMA with a K_i of 0.74 mJ/m^2 [22]. Gabor *et al.* also reported a similar K_i of 0.67 mJ/m^2 in the Ta/Co$_2$FeAl/MgO multilayers even in the as-deposited state [23]. As a result, adding one capping layer on the MgO/Co$_2$FeAl heterostructure not only protects the ferromagnetic layer but also plays an important role in tuning K_i. Consequently, a systematic evaluation of the influence of all the possible metal-based capping layers on K_i of MgO/Co$_2$FeAl heterostructure is of great importance, and so far, there has been no such report.

In this paper, we report a comprehensive study of the interfacial magnetic and energetic properties for the MgO/Co$_2$FeAl interface without and with capping layers, consisting of two sections. In the first section, we consider four types of MgO/Co$_2$FeAl models without capping layers, including MgO/Co$_2$...FeAl, MgO/Co$_2$...Co$_2$, MgO/FeAl...Co$_2$, and MgO/FeAl...FeAl, and investigate their layer-resolved and atomic-orbital-resolved K_i and interfacial cleavage energy. In the second section, we systematically investigate the influence of 26 capping layers on the interfacial K_i of the MgO/Co$_2$...FeAl and MgO/Co$_2$...Co$_2$ systems. Our calculations indicate that adding Fe- and W-capping layers can significantly increase K_i of the system, and particularly, W capping leads to a giant K_i of 4.90 mJ/m^2 in the MgO/Co$_2$...FeAl/W model. This work clarifies the atomistic origin of the interfacial perpendicular magnetic anisotropy at MgO/Co$_2$FeAl, providing some guidance to develop novel p-MTJs with high thermal stability and large K_i.

II. COMPUTATIONAL DETAILS

Density functional theory (DFT) calculations with spin-orbit coupling (SOC) were carried out using the Vienna *Ab initio* Simulation Package (VASP) [24,25]. The projector augmented-wave pseudopotentials were employed for treating electron-ion interactions [26], and the generalized gradient approximation parameterized by the Perdew-Burke-Ernzerhof functional was used for the exchange-correlation functional [27]. The cutoff kinetic energy for plane waves was set

to 450 eV. Γ-centered k-point grids were set to $6 \times 6 \times 1$ and $21 \times 21 \times 1$ for ionic relaxation and static calculations, respectively, which were determined by a careful convergence test for the perpendicular magnetic anisotropy constant K_i, total energy, and cleavage energy of the heterostructure models (see Fig. S1 in the Supplemental Material [28]). The convergence threshold for the electronic self-consistency loop was set to 10^{-6} eV. All the atomic positions and lattice structures were fully relaxed until the residual forces were smaller than 0.02 eV/Å in the structural relaxation. The density of states was calculated using the tetrahedron method with Blöchl corrections [29]. The in-plane lattice constant of the MgO/Co$_2$FeAl heterostructure model was fixed to the lattice constant of MgO (4.215Å).

K_i was calculated by $(E_{[100]} - E_{[001]})/A$, where $E_{[100]}$ and $E_{[001]}$ represent total energy with magnetization along the [100] and [001] directions in a fully self-consistent-field manner, respectively, and A is the in-plane area. It is realized that another approach, i.e., the so-called force theorem, can also be used to calculate K_i, in which a fully self-consistent collinear calculation is required as the first step. After that, noncollinear calculations with magnetization along the [100] and [001] directions are carried out using the frozen charge density produced from the collinear calculation, and then K_i can be calculated based on the energy differences [30]. These two methods generally give consistent results for non-heavy-metal systems, such as Fe/MgO and Fe/MgAl$_2$O$_4$ [31]. However, according to a recent theoretical report, the results might be different for systems with heavy metals, such as Pt and Ir [32]. In this work, to avoid the failure of perturbation theory, the first approach, that is, the fully self-consistent noncollinear SOC calculations, is used for K_i.

III. RESULTS AND DISCUSSION

A. Uncapped MgO/Co$_2$FeAl

We began our study by investigating the interfacial magnetic anisotropy K_i and energetic properties of uncapped MgO/Co$_2$FeAl. Co$_2$FeAl has a cubic crystal structure ($L2_1$) with space group $Fm\bar{3}m$, No. 225 [11,33]. The calculated lattice constants of bulk Co$_2$FeAl and MgO are 5.697 and 4.215 Å, respectively, close to their experimental values of 5.730 and 4.211 Å [33,34]. To match the lattice constant of the MgO substrate, a 45 ° rotation along the [001] direction was made on the conventional lattice structure of Co$_2$FeAl, which yields a lattice mismatch of -4.4%. The negative sign here indicates that the Co$_2$FeAl film undergoes a tensile strain from the MgO substrate. In principle, there are four types of MgO/Co$_2$FeAl slab-based heterostructure models, with all the possible combinations between the two types of MgO/Co$_2$FeAl interfaces (MgO/Co$_2$ and MgO/FeAl interfaces) and two types of Co$_2$FeAl surfaces (with Co$_2$ and FeAl terminations), as shown in Fig. 1. The layers in the Co$_2$FeAl film from the MgO/Co$_2$FeAl interface to the Co$_2$FeAl surface are labeled FL-I to FL-VIII, respectively. For convenience, the heterostructure model consisting of the MgO/Co$_2$ interface and FeAl-terminated surface is referred to as MgO/Co$_2$...FeAl, with similar notation for the other three models, MgO/Co$_2$...Co$_2$, MgO/FeAl...Co$_2$, and MgO/FeAl...FeAl.
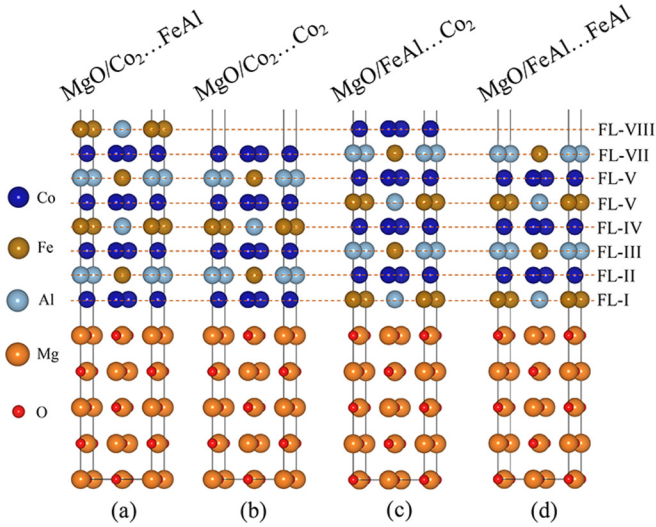
FIG. 1. Schematic crystal structures of uncapped MgO/Co$_2$FeAl heterostructures. (a) MgO/Co$_2$ interface with an FeAl surface (MgO/Co$_2$ . . . FeAl), (b) MgO/Co$_2$ interface with a Co$_2$ surface (MgO/Co$_2$ . . . Co$_2$), (c) MgO/FeAl interface with a Co$_2$ surface (MgO/FeAl . . . Co$_2$), (d) MgO/FeAl interface with an FeAl surface (MgO/FeAl . . . FeAl).

In each model, the Co$_2$FeAl film was built on the MgO substrate with a thickness of five monolayers along the [001] direction, and a vacuum of 15 Å was added on the film to avoid the interaction between images in the periodic lattice. Our test calculations show that increasing the thickness of MgO monolayers to more than five has no effect on the magnetic anisotropy, which is consistent with the prior computational study [21] (see Fig. S2 in the Supplemental Material [28]). It is realized, however, that when the MgO is grown on the ferromagnetic Co$_2$FeAl as overlayers, its thickness could be a crucial factor that influences the magnetic anisotropy of the MgO/Co$_2$FeAl system, according to a recent experimental study [35].

K_i as a function of the thickness of the Co$_2$FeAl film (number of layers) was studied for the four types of heterostructure models, MgO/Co$_2$ . . . FeAl, MgO/Co$_2$ . . . Co$_2$, MgO/FeAl . . . Co$_2$, and MgO/FeAl . . . FeAl. Our calculations show that the calculated K_i generally tends to be saturated when the number of Co$_2$FeAl layers is larger than five for all the types of heterostructure models, as shown in Fig. S3 of the Supplemental Material [28]. This implies there exists a range of film thickness to produce the desired perpendicular magnetic anisotropy. In fact, it was experimentally reported that the critical thickness for the Co$_2$FeAl film to maintain out-of-plane K_i was around 1.1 nm after annealing at 300 °C.[10,36] Therefore, in this work, we choose seven layers (the thickness of the Co$_2$FeAl film is about 0.8 nm) for the MgO/Co$_2$ . . . FeAl and MgO/FeAl . . . Co$_2$ systems and eight layers (about 1 nm) for the MgO/FeAl . . . Co$_2$ and MgO/FeAl . . . FeAl systems to build up the uncapped MgO/Co$_2$FeAl models. Additionally, it is worth noting that the MgO/FeAl . . . FeAl model has a positive K_i (with an easy magnetization axis along the out-of-plane direction) when the Co$_2$FeAl film is ultrathin (one layer), and K_i becomes

TABLE I. Total K_i values of the uncapped MgO/Co$_2$FeAl system with different terminations.

Structure	K_i (mJ/m^2)
MgO/Co$_2$ . . . FeAl	0.60
MgO/Co$_2$ . . . Co$_2$	1.28
MgO/FeAl . . . Co$_2$	0.12
MgO/FeAl . . . FeAl	−1.13

negative (with an easy magnetization axis along the in-plane direction) for multilayers of the Co$_2$FeAl film. The calculated K_i of the MgO/Co$_2$FeAl model with the designated film thickness are 0.60 mJ/m^2 for MgO/Co$_2$ . . . FeAl, 1.28 mJ/m^2 for MgO/Co$_2$ . . . Co$_2$, 0.12 mJ/m^2 for MgO/FeAl . . . Co$_2$, and −1.13 mJ/m^2 for MgO/FeAl . . . FeAl, as listed in Table I. Our calculated K_i of 1.28 mJ/m^2 for the MgO/Co$_2$...Co$_2$ structure is in good agreement with experimental values of 1.04 mJ/m^2 [10] and 1.14 mJ/m^2 [17] and is also very consistent with a recent DFT calculation of 1.31 mJ/m^2 [21].

The effective anisotropy for the MgO/Co$_2$ . . . Co$_2$ model was estimated using the equation [37,38]

$$K_{\mathrm{eff}} t_{\mathrm{eff}} = K_i - \tfrac{1}{2}\mu_0 M_s^2 t_{\mathrm{eff}}, \tag{1}$$

where K_{eff} is the effective anisotropy per unit volume, t_{eff} is the thickness of the ferromagnetic layer, μ_0 is the magnetic constant, and M_s is the saturation magnetization per unit volume. The term $\tfrac{1}{2}\mu_0 M_s^2$ represents the demagnetizing energy per unit volume. In our calculations, the total magnetization for MgO/Co$_2$ . . . Co$_2$ is 17.15μ_B, and the effective thickness is 7.944 Å. Accordingly, the saturation magnetization M_s can be estimated to be 1127 emu/cm^3, which is close to the experimental value of 1140 emu/cm^3 [17]. The term $\tfrac{1}{2}\mu_0 M_s^2 t_{\mathrm{eff}}$ can be estimated to be around 0.63 mJ/m^2, which is much less than the value of K_i considered in this study. Therefore, it is reasonable to conclude that the effective anisotropy still favors the PMA in the MgO/Co$_2$ . . . Co$_2$ model.

To understand the origin of K_i, we calculated layer-resolved K_i for the four types of models, which clearly show the atomic contributions to K_i (see Fig. 2). The layer-resolved K_i was calculated based on the energy difference in noncollinear calculations projected for the atom in each layer. As one can see, the Al atom barely contributes to K_i; however, Co and Fe atoms play an important role in producing K_i. For the models MgO/Co$_2$ . . . FeAl and MgO/Co$_2$ . . . Co$_2$, the two interfacial Co atoms in the FL-I layer contribute most of the out-of-plane K_i, resulting in positive total K_i of 0.60 and 1.28 mJ/m^2, respectively [see Figs. 2(a) and 2(b)]. On the contrary, for the MgO/FeAl . . . Co$_2$ and MgO/FeAl . . . FeAl models, the interfacial Fe atoms (FL-I) and Co atoms (IF-II) cause negative K_i, which explains the relatively low K_i (0.12 mJ/m^2) in MgO/FeAl . . . Co$_2$ and even negative K_i (−1.13 mJ/m^2) in MgO/FeAl . . . FeAl. In the MgO/FeAl . . . Co$_2$ model, the surface Co atoms in the layer FL-VIII cause a large out-of-plane K_i, cancel out the in-plane K_i, and lead to a total positive but low K_i [see Fig. 2(c)]. In the model MgO/FeAl . . . FeAl, almost all the layers contribute in-plane K_i, leading to a total negative K_i [see Fig. 2(d)]. Interestingly, although the MgO/FeAl . . . Co$_2$ and MgO/FeAl . . . FeAl models have the same interface, i.e.,
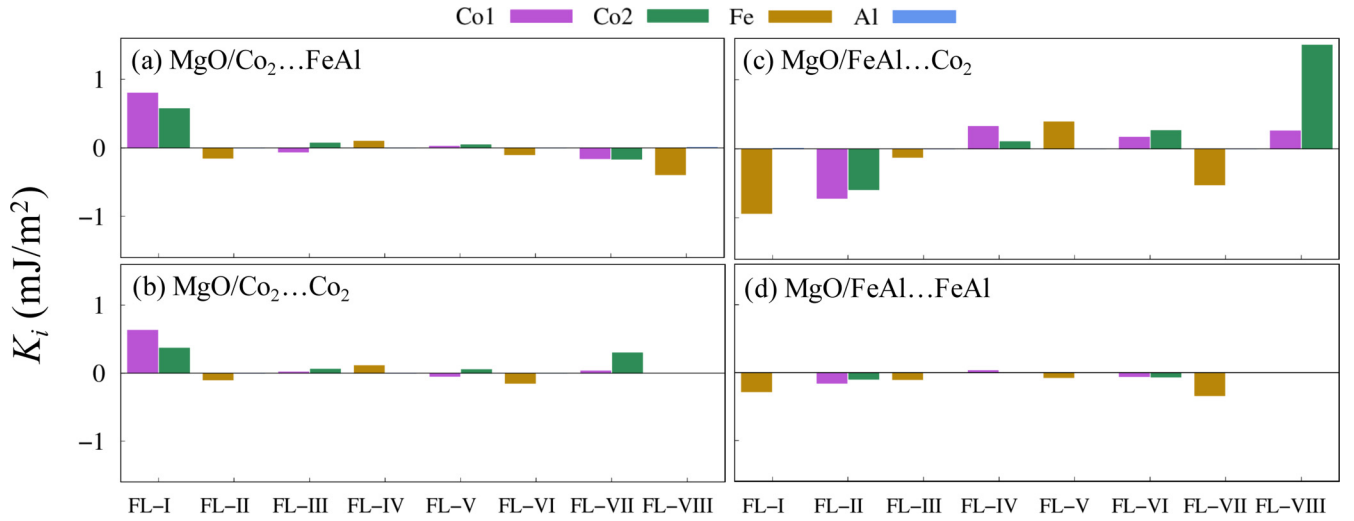
FIG. 2. Calculated layer-resolved K_i values of different atoms for (a) MgO/Co$_2$...FeAl, (b) MgO/Co$_2$...Co$_2$, (c) MgO/FeAl...Co$_2$, and (d) MgO/FeAl...FeAl structures. Labels FL-I to FL-VIII correspond to the layers from the MgO/Co$_2$FeAl interface with the Co$_2$FeAl surface. The purple and green bars represent two different Co atoms in the same layer, while the orange and blue bars indicate the Fe and Al atoms, respectively, in the same layer.

MgO/FeAl, their layer-resolved K_i are significantly different, which may be attributed to the structure symmetry of the Co$_2$FeAl layer [2]. That is, one additional Co$_2$ layer in the MgO/FeAl...Co$_2$ model can significantly change the layer-resolved K_i compared to the MgO/FeAl...FeAl model, in which the ferromagnetic Co$_2$FeAl layer is symmetrical. In short, our calculations reveal that the MgO/Co$_2$ interface produces the out-of-plane K_i, while the MgO/FeAl interface produces in-plane K_i.

To further understand the microscopic origin of K_i, we calculated the orbital-resolved K_i for the interfacial atoms, i.e., Co $3d$ orbitals at the MgO/Co$_2$ interface and Fe $3d$ and Al $3p$ orbitals at the MgO/FeAl interface, as shown in Fig. 3. For the MgO/Co$_2$...FeAl and MgO/Co$_2$...Co$_2$ models, the out-of-plane K_i mainly comes from hybridization between d_{xz} and d_{yz} orbitals of the interfacial Co atoms at the MgO/Co$_2$ interface, around 0.25 and 0.20 mJ/m^2, respectively [see Figs. 3(a) and 3(b)]. The hybridization between d_{z^2} and d_{yz} also contributes to the out-of-plane K_i in both structures; however, the magnitude is much small. For the MgO/FeAl...FeAl and MgO/FeAl...Co$_2$ models, d_{xz} and d_{yz} orbital hybridization of Fe atoms at the MgO/FeAl interface also yields out-of-plane K_i, about 0.37 and 0.08 mJ/m^2, respectively, as shown in Figs. 3(c) and 3(d). However, the orbital hybridization between $d_{x^2-y^2}$ and d_{xy} and $d_{x^2-y^2}$ and d_{yz} leads to an in-plane (negative) K_i and the resulting relatively low out-of-plane total K_i for the MgO/FeAl...Co$_2$ model and even negative K_i for the MgO/FeAl...FeAl model.

The SOC effects on the magnetic anisotropy energy (MAE) can be derived from the second perturbation theory [39]:

$$
\text{MAE} \approx (\xi)^2 \sum_{o^\downarrow, u^\downarrow} \frac{|\langle o^\downarrow | L_z | u^\downarrow \rangle|^2 - |\langle o^\downarrow | L_x | u^\downarrow \rangle|^2}{\epsilon_{u^\downarrow} - \epsilon_{o^\downarrow}}
$$
$$
+ (\xi)^2 \sum_{o^\uparrow, u^\downarrow} \frac{|\langle o^\uparrow | L_x | u^\downarrow \rangle|^2 - |\langle o^\uparrow | L_z | u^\downarrow \rangle|^2}{\epsilon_{u^\downarrow} - \epsilon_{o^\uparrow}}, \quad (2)
$$

where ξ is the SOC constant; $o^\uparrow$ ($u^\uparrow$) and $o^\downarrow$ ($u^\downarrow$) denote the occupied (unoccupied) spin-up and spin-down eigenstates, respectively; $\epsilon_{o^\uparrow(u^\uparrow)}$ and $\epsilon_{o^\downarrow(u^\downarrow)}$ represent eigenvalues of occupied (unoccupied) spin-up and spin-down states, respectively; and L_z (L_x) are the angular momentum operators. This theory has been used to successfully explain the K_i distribution of interfacial Fe over the Brillouin zone in Fe/MgO [40,41], Fe/CuInSe$_2$ [38], Fe/MgAl$_2$O$_4$ [31], and organic/CoFe$_3$N [42]. For a system with a large spin polarization like MgO/Co$_2$FeAl, the coupling effects from the opposite spin channel can be neglected, and thus, the MAE is mainly determined by the coupling between the occupied and unoccupied spin-down states near the Fermi level [39]. In this case, the orbital coupling between occupied and unoccupied states yields a positive K_i if these states share the same quantum number $|m|$, and the coupling yields a negative K_i if the quantum numbers of these states differ by 1. To be specific, the orbital coupling between occupied and unoccupied spin-down states, i.e., d_{xy} and $d_{x^2-y^2}$ (with $|m| = 2$), and between d_{xz} and d_{yz} (with $|m| = 1$) will contribute to a positive K_i [37,43].

To qualitatively understand how the orbital hybridization determines magnetic anisotropy, we calculated the projected density of states of d orbitals for the interfacial Co atom in the MgO/Co$_2$...Co$_2$ model and for the interfacial Fe atom in the MgO/FeAl...FeAl model, as shown in Figs. 4(a) and 4(b), respectively. For the MgO/Co$_2$...Co$_2$ model, spin-down d_{yz} and d_{xz} orbitals contribute both occupied and unoccupied states in the very vicinity (± 0.1 eV) of the Fermi level, and hence, their orbital coupling between occupied and unoccupied states leads to an out-of-plane K_i. This is also consistent with the orbital-resolved K_i in Fig. 3(b). For the MgO/FeAl...FeAl model, the orbital coupling between occupied d_{xz} and unoccupied d_{yz} states leads to positive K_i, as shown in the orbital-resolved K_i in Fig. 3(d), similar to the case for the MgO/Co$_2$...Co$_2$ model. However, as discussed
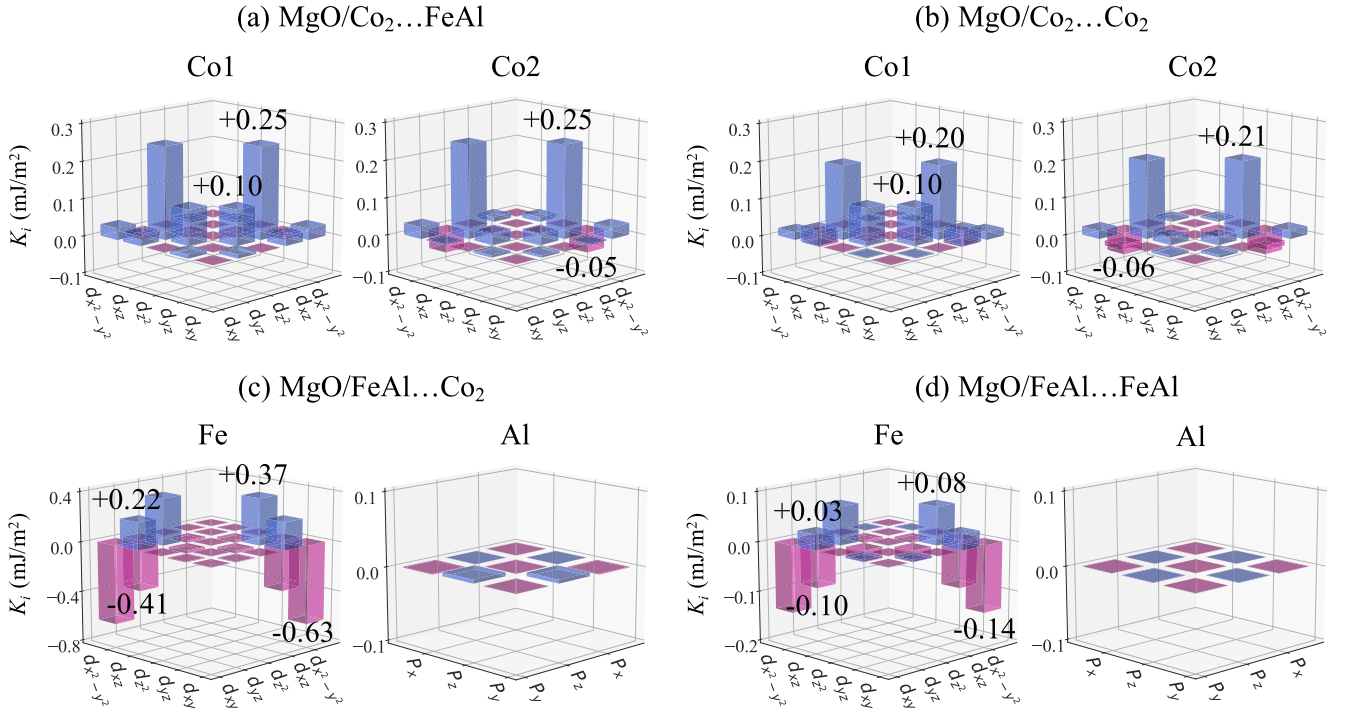
FIG. 3. Calculated atomic-resolved K_i contributions from different orbital hybridizations. (a) and (b) are d-orbital hybridization of interfacial Co atoms in the MgO/Co$_2$...FeAl and MgO/Co$_2$...Co$_2$ structures, respectively. (c) and (d) are d-orbital hybridization of the interfacial Fe atom and p-orbital hybridization of the interfacial Al atom in the MgO/FeAl...Co$_2$ and MgO/FeAl...FeAl structures, respectively.

below, from the k-space-resolved MAE, the orbital coupling between d_{yz} (d_{xz}) and $d_{x^2-y^2}$ states leads to negative K_i, thus resulting in a negative K_i in total.
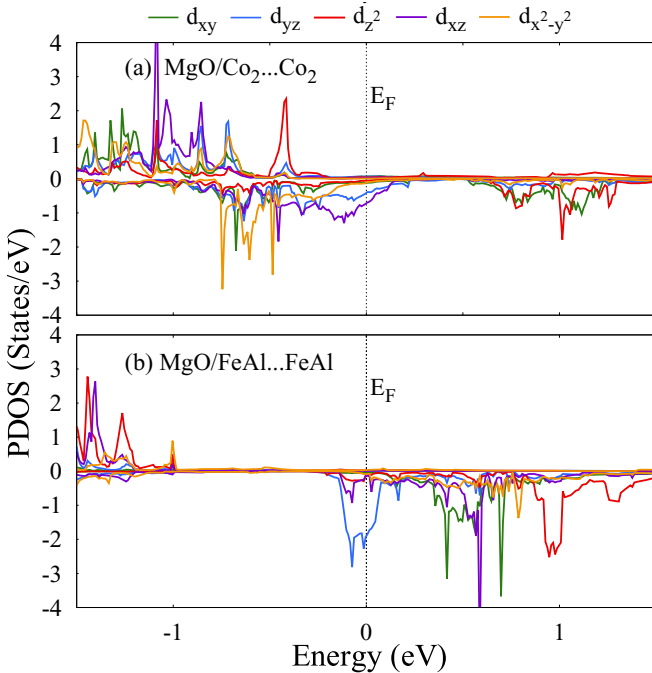
FIG. 4. Calculated projected density of states (PDOS) of d orbitals for (a) the Co$_2$ atom at the MgO/Co$_2$ interface in the MgO/Co$_2$...Co$_2$ model and (b) the Fe atom at the MgO/FeAl interface in the MgO/FeAl...FeAl model.

To deeply understand the relationship between orbital hybridization and magnetic anisotropy, we further calculated the k-space-resolved MAE projected on the two-dimensional interfacial Brillouin zone using the so-called force theorem approach [44] [see Figs. 5(a) and 6(a)]. The d-orbital-projected band structures for the two models, MgO/Co$_2$...Co$_2$ and MgO/FeAl...FeAl, are also shown in Figs. 5(b) and 6(b), respectively. For the MgO/Co$_2$...Co$_2$ model, as shown in Figs. 5(a) and 5(b), its positive MAE at k points 1 and 2 arises from the coupling between occupied and unoccupied spin-down states d_{xz} and d_{yz} along Γ-M and Γ-X, respectively. This conclusion is also in good agreement with our orbital-resolved K_i values for interfacial Co atoms in Fig. 3(b). For the MgO/FeAl...FeAl model, as shown in Figs. 6(a) and 6(b), its positive MAE at k point 1 arises from the coupling between occupied and unoccupied spin-down states d_{xz} and d_{yz} along Γ-X, while the negative MAE at k points 2 and 3 comes from the coupling between occupied and unoccupied spin-down d_{yz} and $d_{x^2-y^2}$ orbitals along Γ-X and between d_{xz} and $d_{x^2-y^2}$ orbitals along Γ-M, respectively.

To evaluate relative interfacial thermal stability, we calculated the cleavage energy of the MgO/Co$_2$ and MgO/FeAl interfaces using the bulk heterostructure model of MgO/Co$_2$FeAl (without vacuum) based on the following equation [45]:

$$E_{\text{cleav.}} = \left(E_{\text{slab}}^{\text{Co}_2\text{FeAl}} + E_{\text{slab}}^{\text{MgO}} - E_{HS}^{\text{MgO/Co}_2\text{FeAl}} \right)/2A, \quad (3)$$

where $E_{\text{slab}}^{\text{Co}_2\text{FeAl}}$, $E_{\text{slab}}^{\text{MgO}}$, and $E_{HS}^{\text{MgO/Co}_2\text{FeAl}}$ are the total energies of the Co$_2$FeAl slab, the MgO slab, and the MgO/Co$_2$FeAl heterostructure, respectively. A is the in-plane interfacial area,
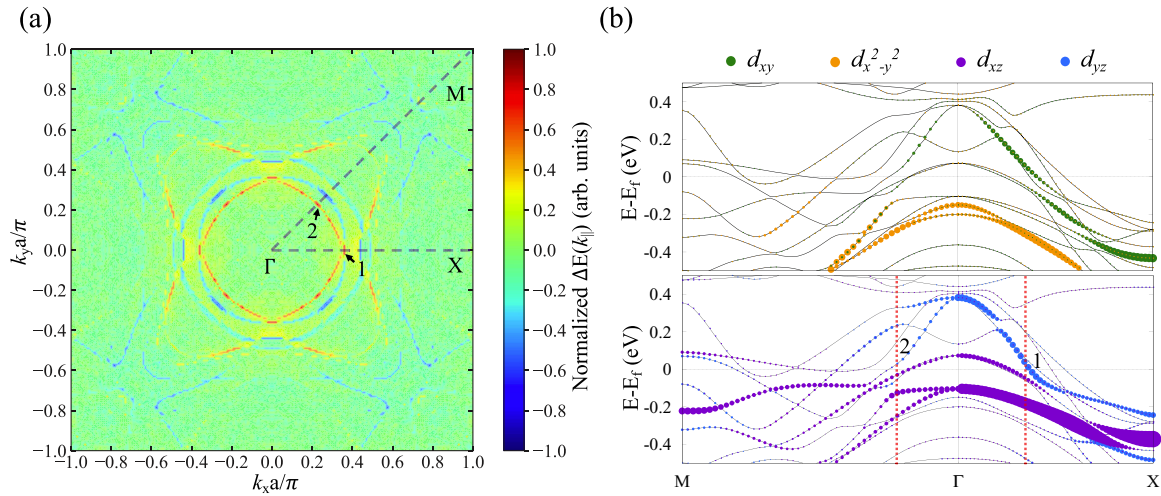
FIG. 5. The k-resolved MAE and d-orbital-projected band structure for the MgO/Co$_2$...Co$_2$ structure. (a) Distribution of the MAE of the interfacial Co atom (the Co atom at the MgO/Co$_2$ interface) in the 2D Brillouin zone. The MAE value was normalized to the maximum positive value of the 2D Brillouin zone. Red and blue represent out-of-plane and in-plane MAEs, respectively. (b) The d-orbital-projected band structure of the interfacial Co atom in spin-down states. The positions of vertical red dashed lines 1 and 2 correspond to the out-of-plane MAE from coupling between d_{xz} and d_{yz} orbitals.

and the factor of 2 in the denominator represents two symmetrical interfaces in the heterostructure model. The calculated cleavage energy was 117 meV/Å^2 for the MgO/Co$_2$ interface and 82 meV/Å^2 for the MgO/FeAl interface, indicating that the MgO/Co$_2$ interface is energetically more favorable than the MgO/FeAl interface. Accordingly, we can conclude that the MgO/Co$_2$ interface is more likely to form than the MgO/FeAl interface in the experiments. Considering the positive K_i at the MgO/Co$_2$ interface and the negative (or close to zero) K_i at the MgO/FeAl interface, this conclusion is also very consistent with the experimentally observed perpen-

dicular magnetic anisotropy at the interface of MgO/Co$_2$FeAl [10,17].

The relative thermal stability of the two interface models can be understood from the interfacial bond length and the resulting bond strength. The local geometrical structures of the two interface models are shown in Fig. 7. The two Co-O bonds at the MgO/Co$_2$ interface are equivalent, with a bond length of 2.05 Å, while at the MgO/FeAl interface, the relaxed Fe-O and Al-O bonds are different mainly because of the different atomic radii for Fe and Al, with a bond length of 2.21 and 2.02 Å, respectively. Accordingly, the relatively low
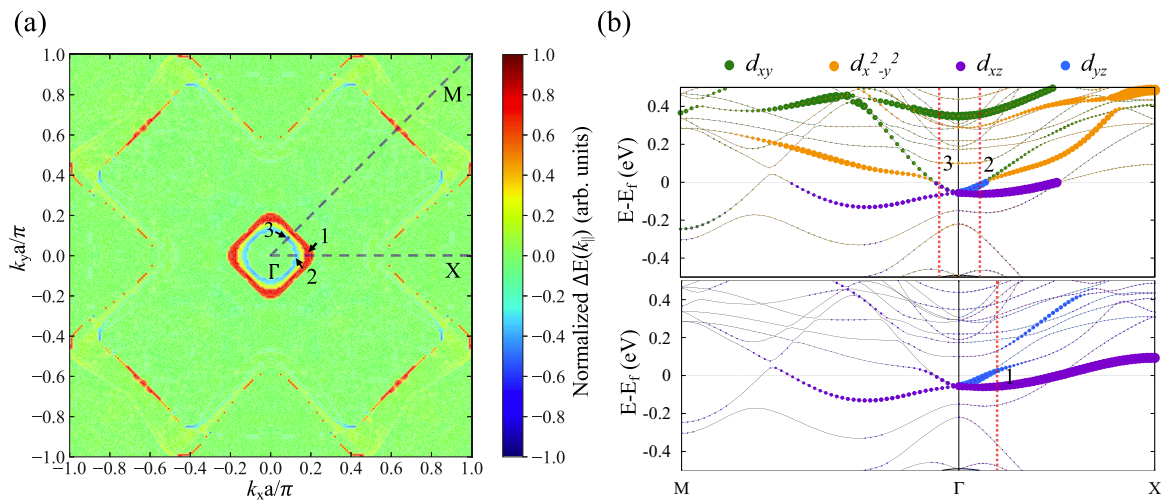

FIG. 6. The k-resolved MAE and d-orbital-projected band structure for the MgO/FeAl...FeAl structure. (a) Distribution of the MAE of the interfacial Fe atom (the Fe atom at the MgO/FeAl interface) in the 2D Brillouin zone. The MAE value was normalized to the maximum positive value of the 2D Brillouin zone. Red and blue represent out-of-plane and in-plane MAEs, respectively. (b) The d-orbital-projected band structure of the interfacial Fe atom in spin-down states. The position of vertical red dashed line 1 corresponds to the out-of-plane MAE from coupling between d_{xz} and d_{yz} orbitals, and the positions of vertical red dashed lines 2 and 3 correspond to the in-plane MAE from coupling between d_{yz} and $d_{x^2-y^2}$ orbitals and coupling between d_{xz} and $d_{x^2-y^2}$ orbitals.
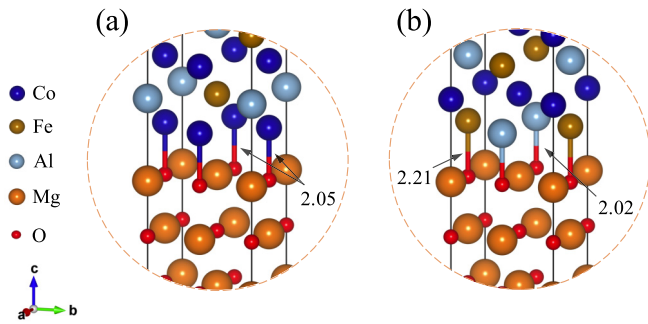
FIG. 7. Schematic illustration of the interfacial bond length (in Å) at (a) the MgO/Co$_2$ interface and (b) the MgO/FeAl interface.

cleavage energy at the MgO/FeAl interface can be attributed to the unmatched Fe-O and Al-O bond length and the resulting relatively weak bond strength, while the highly uniform interfacial structure (equivalent Co-O bonds) at the MgO/Co$_2$ interface leads to relatively high cleavage energy. Note that the unmatched bond strength between the Fe-O and Al-O bonds can also be proven with the Bader charge analysis for the interfacial O atoms [46].

B. Capped MgO/Co$_2$FeAl

In this section, we study the influence of adding capping layers to the interfacial magnetic anisotropy of MgO/Co$_2$FeAl. A total of 26 metal elements, including 3d (Ti, V, Cr, Mn, Fe, Ni, and Cu), 4d (Zr, Nb, Mo, Tc, Ru, Rh, Pd, and Ag), 5d (Hf, Ta, W, Re, Os, Ir, Pt, and Au) transition metals and 6p (Tl, Pb, and Bi) metals, were considered as capping layers. The selection of these elements is based on the consideration that these elements have a relatively large SOC interaction that is likely to be capable of tuning the interfacial magnetic anisotropy [7]. The Co element is not included due to the large lattice mismatch between fcc Co and MgO substrate (∼16%). Since our calculations show that the MgO/Co$_2$ interface is energetically more favorable than the MgO/FeAl interface, here we considered only the MgO/Co$_2$ . . . FeAl and MgO/Co$_2$ . . . Co$_2$ models. We built the capped MgO/Co$_2$FeAl by adding the fcc-type or bcc-type structures of these metal elements on top of the Co$_2$FeAl film while maintaining the thickness of the vacuum around 15 Å (see Fig. 8). It is noted that, for the MgO/Co$_2$ . . . Co$_2$ model, there are two types of interfacial structures between the Co$_2$FeAl film and bcc-type capping layer (including Tl, Pb, and Bi) and one type of interfacial structure between the Co$_2$FeAl film and fcc-type capping layer, as shown in the schematic crystal structures in Fig. 8. The layers of the capping elemental compound are labeled CL-I, CL-II, CL-III, CL-IV, and CL-V, respectively. In the case of V-, Cr-, Mn-, Fe-, Ni-, Cu-, and W-capped structures, to produce the best lattice match, a 45 ° rotation along the [001] direction was made on the conventional bulk structure of bcc-type V, Cr, Mn, Fe, Ni, Cu, and W, leading to only one type of interfacial structure. By taking W-capped MgO/Co$_2$FeAl as one example, we also studied the total K_i as a function of the number of capping layers, as shown in Fig. S2 of the Supplemental Material [28]. Our calculations show that
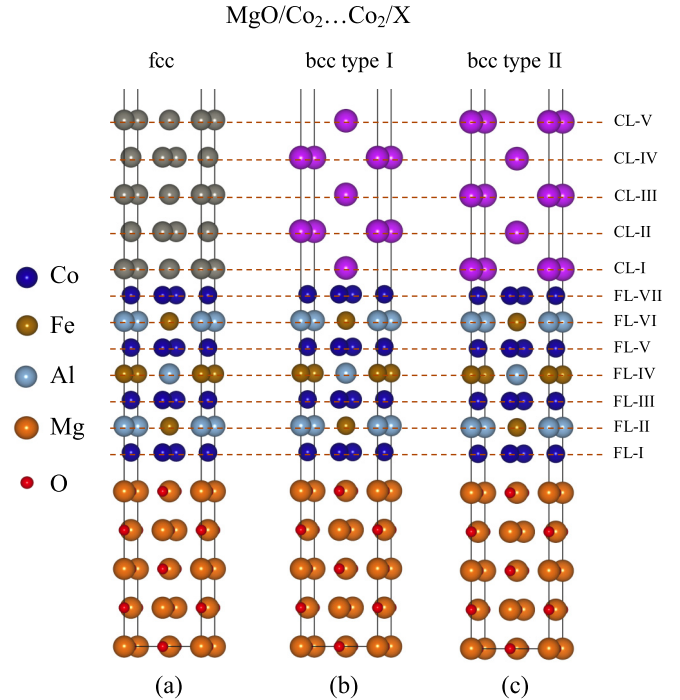

FIG. 8. Schematic crystal structures of capped MgO/Co$_2$ . . . Co$_2$ heterostructure with (a) the fcc structure capping layer, (b) bcc type-I structure capping layer, and (c) bcc type-II structure capping layer.

K_i of the system with an odd number of capping layers (three, five, and seven) is generally larger than that with an even number (four and six); in spite of this, K_i still tends to be saturated as the number of capping layers is larger than five.

Table II shows the summary of K_i values of selected capped MgO/Co$_2$FeAl systems that have a lattice mismatch (between Co$_2$FeAl and capping elemental bulk structure) less than 7%. The detailed results for all 26 capped models are shown in Table S1 of the Supplemental Material [28]. They show that Fe-, Mo-, Pd-, Hf-, W-, and Au-capped MgO/Co$_2$ . . . FeAl structures show a larger K_i of 2.59, 1.37, 1.86, 1.67, 4.90, and 1.82 mJ/m^2 than the uncapped structure. The Tl-, Pb-, and Bi-capped MgO/Co$_2$FeAl structures with a type-II structure also exhibit a large K_i of 2.14, 2.29, and 2.08 mJ/m^2. It is especially worth mentioning that W capping leads to a giant K_i value of 4.90 mJ/m^2 in the MgO/Co$_2$ . . . FeAl/W structure and a K_i of 2.46 mJ/m^2 in the MgO/Co$_2$ . . . Co$_2$/W structure. Interestingly, prior experimental and computational studies indicated that W can also improve K_i in the Fe/W/MgO [7,47] and MgO/CoFeB/W/CoFeB/MgO [48] systems in which a thin W interface layer was inserted as doping. Additionally, our calculation for MgO/Co$_2$ . . . Co$_2$/Ta yields a K_i value of 0.63 mJ/m^2, which is in good agreement with the experimental value of 0.67 mJ/m^2 [23]. To elucidate the origin of the giant K_i in the MgO/Co$_2$ . . . FeAl/W structure, we calculate its layer-resolved K_i and atomic-orbital-resolved K_i in Fig. 9, which clearly shows that the large K_i of MgO/Co$_2$ . . . FeAl/W is mainly contributed by the interfacial W atoms at the CL-I (3.22 mJ/m^2) and CL-II (0.88 mJ/m^2) layers. K_i from the interfacial Co atoms of Co$_2$FeAl is almost

TABLE II. Summary of total K_i values of selected capping elements with lattice mismatch f smaller than 7%. The lattice mismatch is defined as $f = (a_f - a_s)/a_s$, where a_s and a_f are the lattice constants of the substrate and film, respectively. Note that, for the MgO/Co$_2$...Co$_2$/X model (X=Tl, Pb, and Bi), there are two types of interfacial structures (with notations of I and II) between Co$_2$FeAl film and bcc-type capping layers.

X	f (%)	K_i (mJ/m^2)	
		MgO/Co$_2$...FeAl/X	MgO/Co$_2$...Co$_2$/X
Ti	−2.5	0.71	1.00
V	0.4	0.98	0.87
Cr	−4.4	1.20	1.22
Mn	−6.1	0.73	0.48
Fe	−4.4	2.59	2.13
Ni	−6.4	-0.37	1.79
Cu	−3.6	1.21	1.22
Nb	0.4	0.58	1.18
Mo	−4.8	1.37	0.93
Pd	−6.2	1.86	0.60
Ag	−1.3	1.15	1.23
Hf	6.3	1.67	0.93
Ta	0.3	−0.72	0.63
W	6.2	4.90	2.46
Re	−6.9	0.27	−1.63
Pt	−5.6	0.56	−1.37
Au	−1.0	1.82	1.33
Tl (I)	−6.0	−1.76	2.12
Tl (II)			2.14
Pb (I)	−5.0	−0.35	2.01
Pb (II)			2.29
Bi (I)	−5.4	0.40	0.13
Bi (II)			2.08

the same as that in the uncapped MgO/Co$_2$FeAl model, suggesting that the W capping layers have no significant influence on the magnetic anisotropy of the Co$_2$FeAl film but do enhance the total K_i of the MgO/Co$_2$...FeAl/W system. The orbital-resolved K_i of the two interfacial W atoms at the CL-I layer are plotted in Figs. 9(c) and 9(d). These plots show that the out-of-plane K_i largely comes from the d-orbital hybridization between $d_{x^2-y^2}$ and d_{xy} (around 0.50 mJ/m^2) and between d_{xz} and d_{yz} (0.24 mJ/m^2) in both W atoms.

IV. CONCLUSION

In conclusion, we have systematically investigated the interfacial magnetic and energetic properties in the MgO/Co$_2$FeAl heterostructure by modeling four types of interfacial models using first-principles calculations. Our results show that the MgO/Co$_2$ interface can produce out-of-plane K_i, while the MgO/FeAl interface can produce in-plane K_i, and the former interface is energetically more favorable than the latter one and thus is likely to be formed practically. The calculated K_i of 1.28 mJ/m^2 in the MgO/Co$_2$...Co$_2$
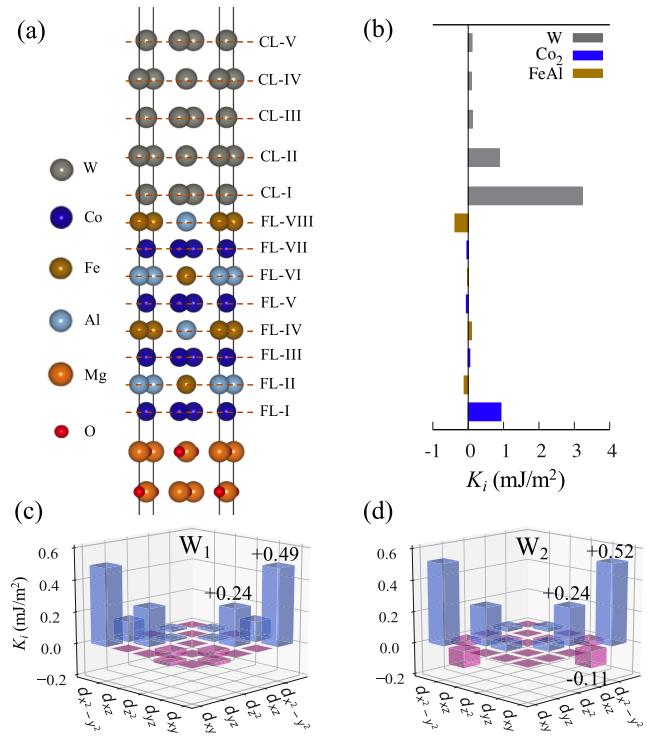

FIG. 9. (a) Schematic crystal structure of W-capped MgO/Co$_2$...FeAl (MgO/Co$_2$...FeAl/W), (b) the layer-resolved K_i value of MgO/Co$_2$...FeAl/W, and (c) and (d) K_i contributions from different d orbital hybridizations at the interfacial atoms of W1 and W2 of MgO/Co$_2$...FeAl/W.

structure is very consistent with the experimental value. In addition, the influence of 26 capping layers on the interfacial magnetic anisotropy was explored. It was found that Fe and W capping can significantly enhance the interfacial K_i in the MgO/Co$_2$FeAl, and particularly, a giant K_i of 4.90 mJ/m^2 can be achieved in the W-capped model. This work reveals the atomistic origin of the large perpendicular magnetic anisotropy at the MgO/Co$_2$FeAl interface and offers insights for tuning interfacial K_i via adding capping layers in the MgO/Co$_2$FeAl.

[1] Y. Huai, AAPPS Bull. **18**, 33 (2008).

[2] A. Khvalkovskiy, D. Apalkov, S. Watts, R. Chepulskii, R. Beach, A. Ong, X. Tang, A. Driskill-Smith, W. Butler, P. Visscher *et al.*, J. Phys. D **46**, 074001 (2013).

[3] A. Moser, K. Takano, D. T. Margulies, M. Albrecht, Y. Sonobe, Y. Ikeda, S. Sun, and E. E. Fullerton, J. Phys. D **35**, R157 (2002).

[4] S. Yuasa, T. Nagahama, A. Fukushima, Y. Suzuki, and K. Ando, Nat. Mater. **3**, 868 (2004).

[5] S. Ikeda, K. Miura, H. Yamamoto, K. Mizunuma, H. D. Gan, M. Endo, S. Kanai, J. Hayakawa, F. Matsukura, and H. Ohno, Nat. Mater. **9**, 721 (2010).

[6] S. Peng, D. Zhu, J. Zhou, B. Zhang, A. Cao, M. Wang, W. Cai, K. Cao, and W. Zhao, Adv. Electron. Mater. **5**, 1900134 (2019).

[7] S. Nazir, S. Jiang, J. Cheng, and K. Yang, Appl. Phys. Lett. **114**, 072407 (2019).

[8] S. Peng, W. Kang, M. Wang, K. Cao, X. Zhao, L. Wang, Y. Zhang, Y. Zhang, Y. Zhou, K. L. Wang, and W. Zhao, IEEE Magn. Lett. **8**, 3105805 (2017).

[9] V. W. Guo, B. Lu, X. Wu, G. Ju, B. Valcu, and D. Weller, J. Appl. Phys. **99**, 08E918 (2006).

[10] Z. Wen, H. Sukegawa, S. Mitani, and K. Inomata, Appl. Phys. Lett. **98**, 242507 (2011).

[11] M. S. Gabor, T. Petrisor, Jr., C. Tiusan, M. Hehn, and T. Petrisor, Phys. Rev. B **84**, 134413 (2011).

[12] A. Kumar, F. Pan, S. Husain, S. Akansel, R. Brucas, L. Bergqvist, S. Chaudhary, and P. Svedlindh, Phys. Rev. B **96**, 224425 (2017).

[13] S. Mizukami, D. Watanabe, M. Oogane, Y. Ando, Y. Miura, M. Shirai, and T. Miyazaki, J. Appl. Phys. **105**, 07D306 (2009).

[14] W. Wang, E. Liu, M. Kodzuka, H. Sukegawa, M. Wojcik, E. Jedryka, G. H. Wu, K. Inomata, S. Mitani, and K. Hono, Phys. Rev. B **81**, 140402(R) (2010).

[15] X. Li, S. Yin, Y. Liu, D. Zhang, X. Xu, J. Miao, and Y. Jiang, Appl. Phys. Express **4**, 043006 (2011).

[16] M. Belmeguenai, H. Tuzcuoglu, M. S. Gabor, T. Petrisor, C. Tiusan, D. Berling, F. Zighem, T. Chauveau, S. M. Chérif, and P. Moch, Phys. Rev. B **87**, 184431 (2013).

[17] A. Conca, A. Niesen, G. Reiss, and B. Hillebrands, J. Phys. D **51**, 165303 (2018).

[18] J. Okabayashi, H. Sukegawa, Z. Wen, K. Inomata, and S. Mitani, Appl. Phys. Lett. **103**, 102402 (2013).

[19] Z. Wen, J. P. Hadorn, J. Okabayashi, H. Sukegawa, T. Ohkubo, K. Inomata, S. Mitani, and K. Hono, Appl. Phys. Express **10**, 013003 (2017).

[20] Z. Bai, L. Shen, Y. Cai, Q. Wu, M. Zeng, G. Han, and Y. P. Feng, New J. Phys. **16**, 103033 (2014).

[21] R. Vadapoo, A. Hallal, H. Yang, and M. Chshiev, Phys. Rev. B **94**, 104418 (2016).

[22] M. Belmeguenai, M. Gabor, T. Petrisor, Jr., F. Zighem, S. Chérif, and C. Tiusan, J. Appl. Phys. **117**, 023906 (2015).

[23] M. S. Gabor, T. Petrisor, C. Tiusan, and T. Petrisor, J. Appl. Phys. **114**, 063905 (2013).

[24] G. Kresse and J. Furthmüller, Comput. Mater. Sci. **6**, 15 (1996).

[25] G. Kresse and J. Furthmüller, Phys. Rev. B **54**, 11169 (1996).

[26] G. Kresse and D. Joubert, Phys. Rev. B **59**, 1758 (1999).

[27] J. P. Perdew, K. Burke, and M. Ernzerhof, Phys. Rev. Lett. **77**, 3865 (1996).

[28] See Supplemental Material at http://link.aps.org/supplemental/10.1103/PhysRevB.101.134405 for the convergence test results for K_i and cleavage energy and the calculated K_i for all 26 capped MgO/Co$_2$FeAl models.

[29] P. E. Blöchl, O. Jepsen, and O. K. Andersen, Phys. Rev. B **49**, 16223 (1994).

[30] S. Steiner, S. Khmelevskyi, M. Marsmann, and G. Kresse, Phys. Rev. B **93**, 224425 (2016).

[31] K. Masuda and Y. Miura, Phys. Rev. B **98**, 224421 (2018).

[32] S. Kwon, Q. Sun, F. Mahfouzi, K. L. Wang, P. K. Amiri, and N. Kioussis, Phys. Rev. Appl. **12**, 044075 (2019).

[33] K. H. J. Buschow, P. G. van Engen, and R. Jongebreur, J. Magn. Magn. Mater. **38**, 1 (1983).

[34] M. Boiocchi, F. Caucia, M. Merli, D. Prella, and L. Ungaretti, Eur. J. Mineral. **13**, 871 (2001).

[35] S. Lakshmanan, M. R. Muthuvel, P. Delhibabu, and H. Annal Therese, Phys. Status Solidi A **215**, 1800316 (2018).

[36] H. Sukegawa, Z. Wen, S. Kasai, K. Inomata, and S. Mitani, Spin **4**, 1440023 (2014).

[37] B. Dieny and M. Chshiev, Rev. Mod. Phys. **89**, 025008 (2017).

[38] K. Masuda, S. Kasai, Y. Miura, and K. Hono, Phys. Rev. B **96**, 174401 (2017).

[39] D.-s. Wang, R. Wu, and A. J. Freeman, Phys. Rev. B **47**, 14932 (1993).

[40] K. Nakamura, T. Akiyama, T. Ito, M. Weinert, and A. J. Freeman, Phys. Rev. B **81**, 220409(R) (2010).

[41] S. Kwon, P.-V. Ong, Q. Sun, F. Mahfouzi, X. Li, K. L. Wang, Y. Kato, H. Yoda, P. K. Amiri, and N. Kioussis, Phys. Rev. B **99**, 064434 (2019).

[42] Z. Li, W. Mi, and H. Bai, ACS Appl. Mater. Interfaces **10**, 16674 (2018).

[43] X. Chen, S. Zhang, B. Liu, F. Hu, B. Shen, and J. Sun, Phys. Rev. B **100**, 144413 (2019).

[44] G. H. O. Daalderop, P. J. Kelly, and M. F. H. Schuurmans, Phys. Rev. B **41**, 11919 (1990).

[45] S. Nazir, M. Behtash, and K. Yang, J. Appl. Phys. **117**, 115305 (2015).

[46] W. Tang, E. Sanville, and G. Henkelman, J. Phys.: Condens. Matter **21**, 084204 (2009).

[47] Y. Iida, Q. Xiang, J. Okabayashi, T. Scheike, H. Sukegawa, and S. Mitani, J. Phys. D **53**, 124001 (2019).

[48] J.-H. Kim, J.-B. Lee, G.-G. An, S.-M. Yang, W.-S. Chung, H.-S. Park, and J.-P. Hong, Sci. Rep. **5**, 16903 (2015).